Lateral-Torsional Buckling of Retrofitted Steel I-Beams Using FRP Sheets

M.Z. Kabir[1,*] and A.E. Seif[1]

Abstract. *This study intends to present an analytical solution of lateral-torsional buckling of an I-beam, which is retrofitted using FRP sheets. The analytical solution is based on calculating the total potential energy and applying the Rayleigh-Ritz method. It is supposed that the FRP sheet can be used on flanges. Therefore, two cases of retrofitting are the I-beam with Top-Bottom retrofitted flanges (TB) and Bottom retrofitted flange Only (BO). It is also assumed that the flange and the FRP sheet are considered as a continuous hybrid element and the Classical Lamination Theory (CLT) can be applied. Subsequently, from the energy method, stiffness parameters of retrofitted sections are produced for both cases of TB and BO and the critical moment is presented for the retrofitted I-beam under positive end moments. Finally, numerical consideration and a parametric study with various fiber angles in a $[+\theta/-\theta]$ laminate sequence are used for both simple and clamped beams under some typical loadings, to inspect the effects of FRP sheets on the development of the lateral-torsional buckling capacity. Moreover, FEM results are produced from numerical models made up of 2D shell elements to verify the analytical solution.*

Keywords: *Lateral-torsional buckling; Rehabilitation using FRP; Steel members; Classical lamination theory; I-beams.*

INTRODUCTION

Environmental causes lead to the corrosion of steel members and reduce their capacity, so they need retrofitting and strengthening. There are some traditional methods to strengthen steel members such as welding or using adhesively bonding steel plates, but using FRP sheets is the newest method to be applied and which appears to be an excellent solution. For an I-beam, FRP sheets can be attached to flanges to develop their capacity and stability. In view of the load carrying capacity, the behavior of steel I-beams retrofitted using FRP sheets was analytically studied by Youssef [1]. Phares et al. [2] used FRP to strengthen steel girder bridges, and the use of GFRP plates for the rehabilitation of composite steel bridges was presented by El Damatty et al. [3].

Apart from that, for thin walled structures, because of slender elements, stability considerations including local and global buckling are important. In

1. *Department of Civil Engineering, Amirkabir University of Technology, Tehran, P.O. Box 15875-4413, Iran.*
*. *Corresponding author. E-mail: mzkabir@aut.ac.ir*

this case, the analytical solutions ware widely presented for steel beams with different cross-sections, loads and boundary conditions. Also, earlier work was mostly concerned with composite sections especially pultruded beams. Cantilever I-beams were considered analytically by Qiao et al. [4], and an I-section composite cantilever beam under eccentric loading was studied by Jaehong Lee and Seung-hye Lee [5].

Now, paying attention to the importance of the stability of steel thin-walled members and the fact that corrosion can significantly reduce their buckling capacity, it seems that a corrosion resistant material, such as FRP, can be used to enhance the local and global buckling capacity. In this case, some experiments were undertaken by Harries et al. [6] in which a concentric axial compression load has been applied to braces with WT sections to investigate the ability of an FRP retrofit to affect buckling behavior. Also, Accord and Earls [7] studied the ductility enhancement of steel I-beams using a GFRP strip, both experimentally and numerically, and then, showed that the addition of longitudinally oriented GFRP strips to the compression flange of cantilevered steel beams effectively braces the constituent cross sectional plate components against the occurrence of local buckling

during plastic hinging, thereby, increasing the structural ductility and energy dissipation capacity of the member.

However, the deficiency of analytical investigations for the stability of retrofitted steel beams using composite materials is clear, especially for lateral buckling. Thus, the stability analysis of retrofitted steel members can be considered as a great contribution to this field. Since the I-section is an applicable shape for steel beams, this study intends to present an analytical solution of the lateral-torsional buckling of an I-section simple beam; retrofitted using FRP sheets.

KINEMATICS

For the lateral-torsional buckling analysis of retrofitted steel I-beams using FRP sheets, the following assumptions were made:

1. A cross section behaves as a thin-walled section after retrofitting as before.

2. Complete bonding between steel and FRP is always considered and the adhesive thickness was neglected.

3. The retrofitting fabric is applied to one or both flanges.

One global Cartesian coordinate system is used in which x and y orientations are parallel to both major and minor axes of the cross-section, thus, z orientation corresponds to the beam axis. Also, the origin of the coordinate system is located at the centroid of the cross-section (Figure 1). Then, buckling deformation can be specified by the original displacements, U and V, in directions x and y, and rotation ϕ about the z axis as shown in Figure 1.

Transformations Relation

Assuming that only the bottom flange is retrofitted (case BO), the shear center is then moved to a distance
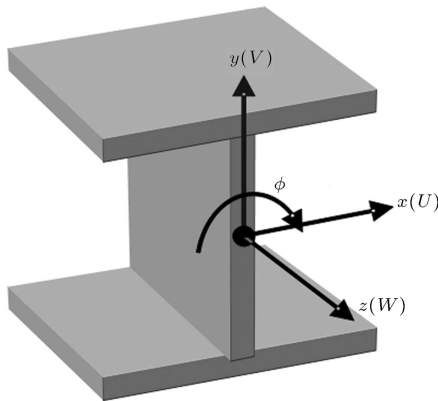
of (a) below the centroid of the cross-section. Thus, transformation of each point of the cross-section can be determined by the following equations [8]:

$$u = U + (y + a)\phi, \tag{1-1}$$

$$v = V - x\phi, \tag{1-2}$$

$$w = -xU' - yV' - \omega\phi', \tag{1-3}$$

where u, v and w are components of transformation in x, y and z directions, respectively. Also, ω indicates a "warping function" and is equal to $x(y + a)$. Now, supposing that both top and bottom flanges are retrofitted in a symmetric manner (case TB), the shear center coincides with the centroid of the cross-section so that $(a = 0)$.

Stiffness Matrix of Hybrid Element

A hybrid element consists of composite and metal components (Figure 2). Based on the CLT theory, the general form of stiffness matrix, S^k, for the kth component of the laminate composite is expressed as:

$$S^k = \begin{bmatrix} A^k & B^k \\ B^k & D^k \end{bmatrix}, \tag{2}$$

where, A^k, D^k and B^k are extensional, bending and bending-extension coupling stiffness matrices and are derived by [9]:

$$A_{ij}^k = \sum_{n=1}^{N} t_n \bar{Q}_{ij}^n,$$

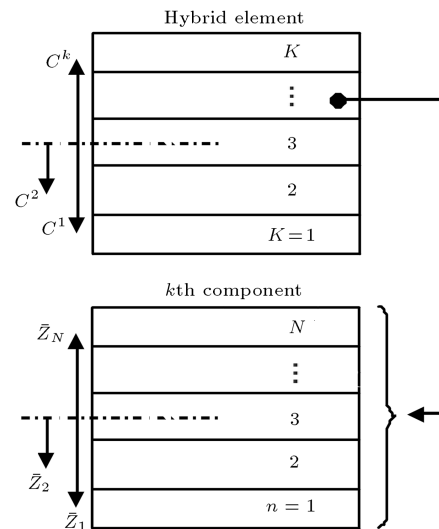$$B_{ij}^k = \sum_{n=1}^{N} -t_n \bar{Z}_n \bar{Q}_{ij}^n,$$

Figure 1. Coordinate system and transformations.

Figure 2. Hybrid element including some composite and metal components.

$$D_{ij}^k = \sum_{n=1}^{N} \left(t_n \bar{Z}_n^2 + \frac{t_n^3}{12} \right) \bar{Q}_{ij}^n. \tag{3}$$

In the above equation, $\bar{Q}_{ij}^n$ are the components of the transformed reduced stiffness matrix of the layup, n. Also, t_n and $\bar{Z}_n$ are the thickness and position of nth layups as shown in Figure 2. Now, the position of the nth layup of the kth component in the hybrid element is derived by:

$$Z_n^H = \bar{Z}_n^H + C^k, \tag{4}$$

where the letter H denotes the hybrid element. Based on the CLT theory, the extensional stiffness matrix will be obtained as follows:

$$(A_{ij}^k)_H = \sum_{n=1}^{N} t_n \bar{Q}_{ij}^n = A_{ij}^k. $$

Thus:

$$A_{ij}^H = \sum_{k=1}^{K} (A_{ij}^k)_H = \sum_{k=1}^{K} A_{ij}^k. \tag{5}$$

Similarly, the bending-extension coupling stiffness matrix is expressed as:

$$(B_{ij}^k)_H = \sum_{n=1}^{N} -t_n \bar{Z}_n^H \bar{Q}_{ij}^n = \sum_{n=1}^{N} -t_n (\bar{Z}_n^k + C^k) \bar{Q}_{ij}^n. $$

Then:

$$B_{ij}^H = \sum_{k=1}^{K} (B_{ij}^k)_H = \sum_{k=1}^{K} B_{ij}^k - C^k A_{ij}^k. \tag{6}$$

Also, the bending stiffness matrix of the hybrid element is written as:

$$(D_{ij}^k)_H = \sum_{n=1}^{N} \left(t_n (\bar{Z}_n^H)^2 + \frac{t_n^3}{12} \right) \bar{Q}_{ij}^n$$

$$= \sum_{n=1}^{N} \left[t_n \left(\bar{Z}_n^k + C^k \right)^2 + \frac{t_n^3}{12} \right] \bar{Q}_{ij}^n$$

$$= \sum_{n=1}^{N} \left[t_n \left(\bar{Z}_n^{k^2} + 2C^k + (C^k)^2 \right) + \frac{t_n^3}{12} \right] \bar{Q}_{ij}^n. $$

Therefore:

$$D_{ij}^H = \sum_{k=1}^{K} \left(D_{ij}^k \right)_H = \sum_{k=1}^{K} D_{ij}^k - 2C^k B_{ij}^k + (C^k)^2 A_{ij}^k. \tag{7}$$

Equations 5 to 7 represent general forms of the hybrid elements stiffness matrices A_{ij}^H, B_{ij}^H and D_{ij}^H in terms of the components' stiffness matrices A_{ij}^k, B_{ij}^k
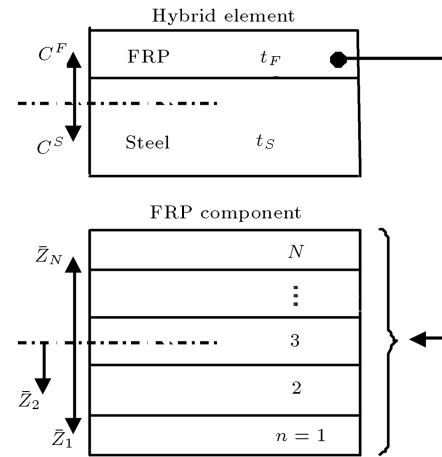

Figure 3. Hybrid element can include some composite and metal components.

and D_{ij}^k and their position in the hybrid element, C^k. Now, in the case of the steel flange retrofitted, using FRP composite fabric, there is a hybrid element compound of two components including FRP and metal (Figure 3).

According to Figure 3, since t_F and t_S are thicknesses of FRP and steel components, their position in the hybrid element are $C^F = t_S/2$ and $C^S = -t_F/2$, respectively. Stiffness matrices of FRP consist of A^F, B^F and D^F and can be determined by CLT theory and Equation 8.

$$A_{ij}^F = \sum_{n=1}^{N} t_n \bar{Q}_{ij}^n,$$

$$B_{ij}^F = \sum_{n=1}^{N} -t_n \bar{Z}_n \bar{Q}_{ij}^n,$$

$$D_{ij}^F = \sum_{n=1}^{N} \left(t_n \bar{Z}_n^2 + \frac{t_n^3}{12} \right) \bar{Q}_{ij}^n. \tag{8}$$

Subsequently, for steel components we have $B_{ij}^S = 0$ and the membrane and flexural stiffness of the metal portion is well known as:

$$A^S = \begin{bmatrix} A_{11}^S & v_S A_{11}^S & 0 \\ v_S A_{11}^S & A_{11}^S & 0 \\ 0 & 0 & A_{33}^S \end{bmatrix},$$

$$D^S = \begin{bmatrix} D_{11}^S & v_S D_{11}^S & 0 \\ v_S D_{11}^S & D_{11}^S & 0 \\ 0 & 0 & D_{33}^S \end{bmatrix},$$

Table 1. Terms of stiffness matrix of hybrid element.

Hybrid	Steel	FRP	Combined
A_{ij}^H	A_{ij}^S	A_{ij}^F	–
B_{ij}^H	–	B_{ij}^F	$A_{ij}^S \frac{t_F}{2} - A_{ij}^F \frac{t_S}{2}$
D_{ij}^H	D_{ij}^S	D_{ij}^F	$A_{ij}^S \frac{t_F^2}{4} + A_{ij}^F \frac{t_S^2}{4} - t_s B_{ij}^F$

$$A_{11}^S = \frac{E_S t_S}{1 - v_S^2}, \qquad A_{33}^S = G_S t_S,$$

$$D_{11}^S = \frac{E_S t_S^3}{12(1 - v_S^2)}, \qquad D_{33}^S = \frac{G_S t_S^3}{12}. \qquad (9)$$

From Equations 5 to 9, the stiffness matrices of the hybrid element shown in Figure 3 will be obtained in which each component of the stiffness matrix includes two terms of steel and FRP, and one combined term as presented in Table 1.

ANALYTICAL ALGORITHM

In this section, the energy criterion is used to determine the lateral-torsional buckling load of a beam based on the internal strain energy and the external work of the load. Since U_i and W_e represent the internal strain energy and the external work of the load, the total potential energy Π will be:

$$\Pi = U_i - W_e. \qquad (10)$$

The internal strain energy of the beam is given by the summation of each element's internal strain energy, and can be determined as follows.

Top and Bottom Flanges

Each flange with a width of b rests on the XZ-plane, and non-zero stress resultants of flanges are shown in Figure 4. Thus, the strain energy of flange U_f is:
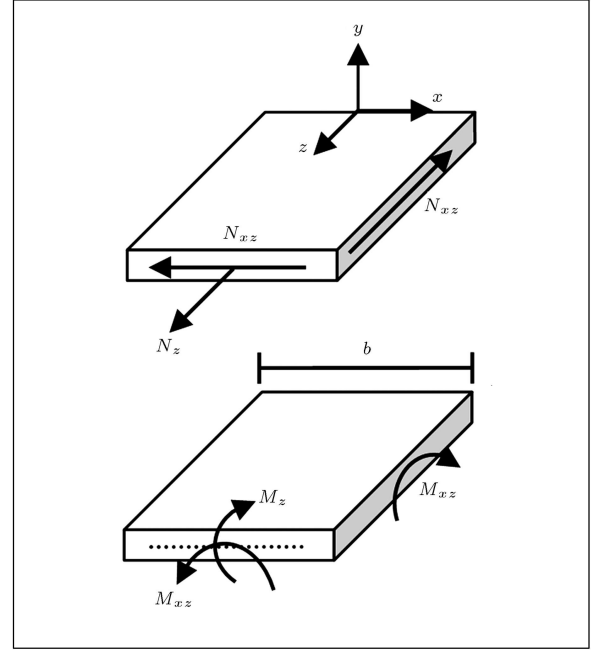
$$U_f = \frac{1}{2} \int_0^L \int_{-b/2}^{b/2} [N_z \varepsilon_z + N_{xz} \gamma_{xz} + M_z k_z$$

$$+ M_{xz} k_{xz}] dx. \qquad (11)$$

Since the linear strains and curvatures are:

$$\varepsilon_z = \frac{\partial w}{\partial z} = -xU'' - yV'' - \omega \phi'', \qquad (12\text{-}1)$$

$$\gamma_{xz} = \frac{\partial w}{\partial x} + \frac{\partial u}{\partial z} = 0, \qquad (12\text{-}2)$$

$$k_z = \frac{\partial^2 v}{\partial z^2} = V'' - x\phi'', \qquad (12\text{-}3)$$

Figure 4. Non-zero stress resultants of flanges.

$$k_{xz} = 2\frac{\partial^2 v}{\partial x \partial z} = -2\phi'. \qquad (12\text{-}4)$$

For retrofitted flanges, a constitutive relation of the hybrid element is used and written as follows with respect to the defined stiffness as tabulated in Table 1.

$$\begin{Bmatrix} N_z \\ N_x \\ N_{xz} \\ M_z \\ M_x \\ M_{xz} \end{Bmatrix} = \begin{bmatrix} A_{11}^H & A_{12}^H & A_{13}^H & B_{11}^H & B_{12}^H & B_{13}^H \\ & A_{22}^H & A_{23}^H & B_{12}^H & B_{22}^H & B_{23}^H \\ & & A_{33}^H & B_{13}^H & B_{23}^H & B_{33}^H \\ & & & D_{11}^H & D_{12}^H & D_{13}^H \\ & & & & D_{22}^H & D_{23}^H \\ sym. & & & & & D_{33}^H \end{bmatrix}$$

$$\cdot \begin{Bmatrix} \varepsilon_z \\ \varepsilon_x \\ \gamma_{xz} \\ k_z \\ k_x \\ k_{xz} \end{Bmatrix}. \qquad (13)$$

It is necessary to note that for the flange, $N_x = M_x = 0$; thus by solving two equations, ε_x and k_x can be derived as follows:

$$\begin{Bmatrix} \varepsilon_x \\ k_x \end{Bmatrix} = - \begin{bmatrix} A_{22}^H & B_{22}^H \\ B_{22}^H & D_{22}^H \end{bmatrix}^{-1}$$

$$\cdot \begin{bmatrix} A_{12}^H & A_{23}^H & B_{12}^H & B_{23}^H \\ B_{12}^H & B_{23}^H & D_{12}^H & D_{23}^H \end{bmatrix} \cdot \begin{Bmatrix} \varepsilon_z \\ \gamma_{xz} \\ k_z \\ k_{xz} \end{Bmatrix}. \qquad (14)$$

By eliminating ε_x and k_x from Equation 13, the reduced stiffness matrix is presented by:

$$\left\{\begin{array}{c} N_z \\ N_{xz} \\ M_z \\ M_{xz} \end{array}\right\} = \begin{bmatrix} A_{11}^* & A_{13}^* & B_{11}^* & B_{13}^* \\ & A_{33}^* & B_{13}^* & B_{33}^* \\ & & D_{11}^* & D_{13}^* \\ Sym. & & & D_{33}^* \end{bmatrix} \cdot \left\{\begin{array}{c} \varepsilon_z \\ \gamma_{xz} \\ k_z \\ k_{xz} \end{array}\right\}, \quad (15)$$

where:

$$\begin{bmatrix} A_{11}^* & A_{13}^* & B_{11}^* & B_{13}^* \\ & A_{33}^* & B_{13}^* & B_{33}^* \\ & & D_{11}^* & D_{13}^* \\ Sym. & & & D_{33}^* \end{bmatrix} =$$

$$\begin{bmatrix} A_{11}^H & A_{13}^H & B_{11}^H & B_{13}^H \\ & A_{33}^H & B_{13}^H & B_{33}^H \\ & & D_{11}^H & D_{13}^H \\ Sym. & & & D_{33}^H \end{bmatrix}$$

$$- \begin{bmatrix} A_{12}^H & B_{12}^H \\ A_{23}^H & B_{23}^H \\ B_{12}^H & D_{12}^H \\ B_{23}^H & D_{23}^H \end{bmatrix} \cdot \begin{bmatrix} A_{22}^H & B_{22}^H \\ B_{22}^H & D_{22}^H \end{bmatrix}^{-1}$$

$$\cdot \begin{bmatrix} A_{12}^H & A_{23}^H & B_{12}^H & B_{23}^H \\ B_{12}^H & B_{23}^H & D_{12}^H & D_{23}^H \end{bmatrix}.$$

For the virgin metal flange, constitutive equations are:

$$\left\{\begin{array}{c} N_z \\ N_{xz} \\ M_z \\ M_{xz} \end{array}\right\} = \begin{bmatrix} t_S E_S & 0 & 0 & 0 \\ & t_S E_S & 0 & 0 \\ & & \frac{t_S^3}{12} E_S & 0 \\ Sym. & & & \frac{t_S^3}{12} G_S \end{bmatrix}$$

$$\cdot \left\{\begin{array}{c} \varepsilon_z \\ \gamma_{xz} \\ k_z \\ k_{xz} \end{array}\right\}, \quad (16)$$

where E_S and G_S are the elastic modulus and shear modulus of steel, and t_S is the flange thickness.

Web

For a web with a height of h and a thickness of t_W, which rests on the xy-plane, non-zero stress resultants are shown in Figure 5.

Accordingly, the strain energy of the web, U_W, including the existent force is:

$$U_W = \frac{1}{2} \int_0^L \int_{-h/2}^{h/2} [N_z \varepsilon_z + N_{yz} \gamma_{yz} + M_z k_z$$

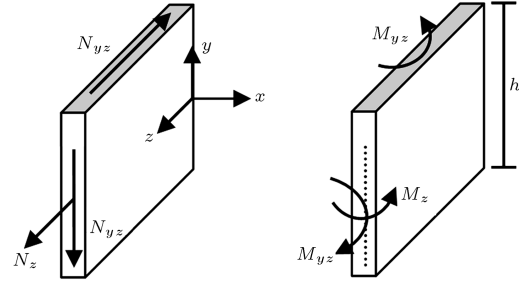$$+ M_{yz} k_{yz}] \, dy \, dz. \quad (17)$$

Figure 5. Non-zero stress resultants of the web.

For the web $x = \omega = 0$, the strains in Equation 17 are calculated as:

$$\varepsilon_z = \frac{\partial w}{\partial z} = -yV'', \quad (18\text{-}1)$$

$$\gamma_{yz} = \frac{\partial w}{\partial y} + \frac{\partial v}{\partial z} = 0, \quad (18\text{-}2)$$

$$k_z = \frac{\partial^2 u}{\partial z^2} = U'' + y\phi'', \quad (18\text{-}3)$$

$$k_{yz} = 2\frac{\partial^2 u}{\partial y \partial z} = 2\phi.' \quad (18\text{-}4)$$

Now for the web, the constitutive relation becomes:

$$\left\{\begin{array}{c} N_z \\ N_{yz} \\ M_z \\ M_{yz} \end{array}\right\} = \begin{bmatrix} t_w E_S & 0 & 0 & 0 \\ & t_w E_S & 0 & 0 \\ & & \frac{t_w^3}{12} E_S & 0 \\ Sym. & & & \frac{t_w^3}{12} G_S \end{bmatrix}$$

$$\cdot \left\{\begin{array}{c} \varepsilon_z \\ \gamma_{yz} \\ k_z \\ k_{yz} \end{array}\right\}. \quad (19)$$

I-BEAM WITH TOP-BOTTOM RETROFITTED FLANGES (CASE TB)

In this case, FRP is applied to both top and bottom flanges, symmetrically, as shown in Figure 6.

By substituting Equations 12 and 15 into Equation 11, the strain energy of the top and bottom flanges is obtained:

$$U_{tf} = \frac{1}{2} \int_0^L \left[(I_y)_{tf} (U'')^2 + (I_x)_{tf} (V'')^2 \right.$$

$$+ (I_\phi)_{tf} (\phi'')^2 + (G)_{tf} (\phi')^2 + (I_{y\phi})_{tf} (U''\phi'')$$

$$\left. + 4(H_{x\phi})_{tf} (V''\phi') \right] dz. \quad (20)$$
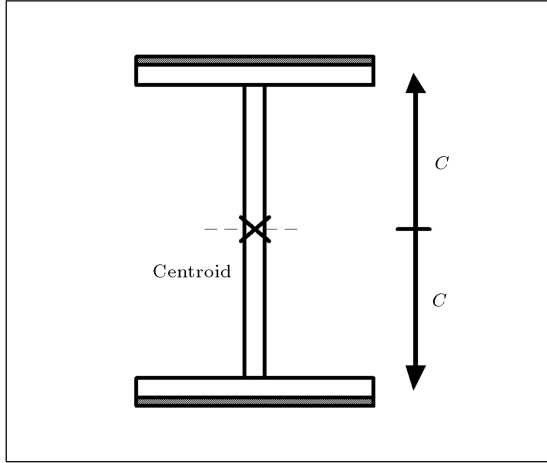
Similarly, the strain energy of the bottom flange is:

Figure 6. I-beam; both flanges are retrofitted.

$$U_{bf} = \frac{1}{2} \int_0^L \big[(I_y)_{bf}(U'')^2 + (I_x)_{bf}(V'')^2$$

$$+ (I_\phi)_{bf}(\phi'')^2 + (G)_{bf}(\phi')^2 + (I_{y\phi})_{bf}(U''\phi'')$$

$$+ 4(H_{x\phi})_{bf}(V''\phi')\big] \, dz. \tag{21}$$

It is necessary to note that in the case of TB, the following relations exist between the rigidities of the top and bottom flanges:

$$(I_y)_{bf} = (I_y)_{tf}, \qquad (I_x)_{bf} = (I_x)_{tf},$$

$$(I_\phi)_{bf} = (I_\phi)_{tf}, \qquad (I_{y\phi})_{bf} = (I_{y\phi})_{tf},$$

$$(G)_{bf} = (G)_{tf}, \qquad (H_{x\phi})_{bf} = (H_{x\phi})_{tf}.$$

Subsequently, using Equations 17-19 will lead to the strain energy of the web.

$$U_w = \frac{1}{2} \int_0^L \big[(I_y)_w(U'')^2 + (I_x)_w(V'')^2$$

$$+ (I_\phi)_w(\phi'')^2 + (G)_w(\phi')^2 \big] \, dz. \tag{22}$$

Now, a summation of the strain energy of beams elements will result in the internal strain energy of the whole beam as:

$$U_i = U_{tf} + U_{bf} + U_w. \tag{23}$$

Substituting Equations 20-22 into Equation 23, the internal strain energy is simplified as in the following expression:

$$U_i = \frac{1}{2} \int_0^L \big[I_y(U'')^2 + I_x(V'')^2 + I_\phi(\phi'')^2$$

$$+ G(\phi')^2 + 4H_{x\phi}(V''\phi')\big] \, dz, \tag{24}$$

in which the stiffness parameters are defined as:

$$I_y = \frac{b^3}{6}(A_{11}^*) + \frac{ht_w^3}{12}E_s,$$

$$I_x = 2b(A_{11}^*C^2 - 2B_{11}^*C + D_{11}^*) + \frac{t_w h^3}{12}E_s,$$

$$I_\phi = \frac{b^3}{6}(A_{11}^*C^2 + 2B_{11}^*C + D_{11}^*) + \frac{h^3 t_w^3}{144}E_s,$$

$$G = 8bD_{33}^* + \frac{ht_w^3}{12}G_s,$$

$$H_{x\phi} = 2b(B_{13}^*C - D_{13}^*).$$

I-BEAM WITH BOTTOM RETROFITTED FLANGE ONLY (CASE BO)

The Centroid of the Cross-Section

Both the centroid and the shear-center of the beam with bottom retrofitted flange only are presented in Figure 7.

Figure 8 shows the external force, P, which is located at the centroid and is balanced by internal stress resultants. Hence, there is a constant strain, ε_z, for the section and no curvature is generated.

For the bottom flange, strains can be obtained from Equation 13. Then in this case, $k_z = 0$, the
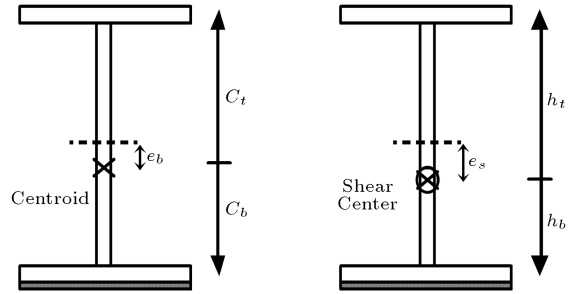

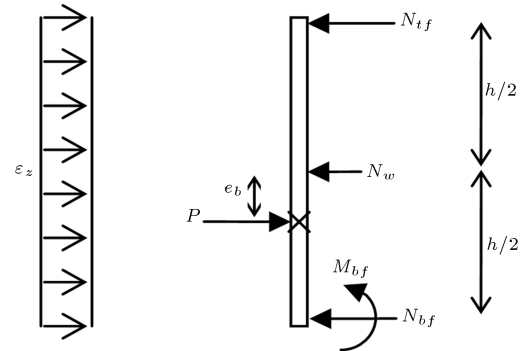**Figure 7.** I-beam with bottom retrofitted flange only.

Figure 8. Internal stress resultants balanced by the external force at centroid.

following relation is derived.

$$
\begin{Bmatrix} \varepsilon_z \\ \varepsilon_x \\ \gamma_{xz} \\ 0 \\ k_x \\ k_{xz} \end{Bmatrix} = \begin{bmatrix} a_{11} & a_{12} & a_{13} & b_{11} & b_{12} & b_{13} \\ & a_{22} & a_{23} & b_{12} & b_{22} & b_{23} \\ & & a_{33} & b_{13} & b_{23} & b_{33} \\ & & & d_{11} & d_{12} & d_{13} \\ & & & & d_{22} & d_{23} \\ sym. & & & & & d_{33} \end{bmatrix}
$$

$$
\cdot \begin{Bmatrix} N_{bf} \\ 0 \\ 0 \\ M_{bf} \\ 0 \\ 0 \end{Bmatrix}. \tag{25}
$$

One can simplify:

$$
\varepsilon_z = a_{11}N_{bf} + b_{11}M_{bf}, \qquad 0 = b_{11}N_{bf} + d_{11}M_{bf}.
$$

Thus:

$$
N_{bf} = \left(\frac{d_{11}}{a_{11}d_{11} - b_{11}^2} \right) \varepsilon_z, \tag{26}
$$

$$
M_{bf} = \left(\frac{b_{11}}{d_{11}} \right) \varepsilon_z. \tag{27}
$$

Now, writing equilibrium equations and eliminating P will lead to:

$$
e_b = \frac{b \left(\frac{d_{11}}{a_{11}d_{11} - b_{11}^2} \right) \left(\frac{h}{2} + \frac{b_{11}}{d_{11}} \right) - E_s \left(t_s b \frac{h}{2} \right)}{b \left(\frac{d_{11}}{a_{11}d_{11} - b_{11}^2} \right) + E_s \left(t_s b + t_w h \right)}, \tag{28}
$$

where t_w and t_S are the thicknesses of the web and flange, since h and b are the height of the web and the flange thickness. Assuming $b_{11} = 0$, the above equation can then be simplified as below:

$$
e_b = \left(\frac{t_0 - t_s}{t_0 + t_s + t_w \frac{h}{2}} \right) \frac{h}{2}, \tag{29}
$$

$$
t_0 = \frac{1}{E_s a_{11}}. \tag{30}
$$

The centers of the top and bottom flanges from the section centroid are:

$$
C_t = \frac{h}{2} + e_b, \qquad C_b = \frac{h}{2} - e_b. \tag{31}
$$

Shear Center

The distance between the shear center and bottom flange, h_b (see Figure 7), for a mono-symmetric I-beam is given by [10]:

$$
h_b = \left[\frac{(I_y)_{tf}}{Iy} \right] h, \tag{32}
$$

where $(I_y)_{tf}$ and I_y are the second moment of the top flange and the cross section about the y-axis. Since the width of both flanges is equal, neglecting web thickness will lead to a simplified equation:

$$
h_b = \left(\frac{t_s}{t_0 + t_s} \right) h. \tag{33}
$$

Also for the top flange:

$$
h_t = \left(\frac{t_0}{t_0 + t_s} \right) h. \tag{34}
$$

Now, the deflection of the shear center, e_s, is given by:

$$
e_s = \frac{h}{2} - h_b. \tag{35}
$$

Thus, the difference between the centroid and the shear center is:

$$
a = e_s - e_b. \tag{36}
$$

Strain Energy

Similar to part 4, in the case of BO, summation of the strain energy of beam elements will lead to the strain energy of the beam.

$$
U_i = \frac{1}{2} \int_0^L \left[I_y(U'')^2 + I_x(V'')^2 + I_\phi(\phi'')^2 \right.
$$
$$
\left. + G(\phi')^2 + 2I_{y\phi}(U''\phi'') + 4H_{x\phi}(V''\phi') \right] dz, \tag{37}
$$

in which the stiffness parameters are defined as:

$$
I_y = \frac{b^3}{12}(A_{11}^*) + \left[\frac{t_s b^3}{12} + \frac{h\, t_w^3}{12} \right] E_s,
$$

$$
I_x = b(A_{11}^* C_b^2 - 2B_{11}^* C_b + D_{11}^*)
$$
$$
+ \left[bt_s C_t^2 + \frac{t_w}{3}(C_b^3 + C_t^3) \right] E_s,
$$

$$
I_\phi = \frac{b^3}{12}(A_{11}^* h_b^2 + 2B_{11}^* h_b + D_{11}^* + E_s t_s h_t^2),
$$

$$
G = 4bD_{33}^* + \left[\frac{bt_s^3}{3} + \frac{ht_w^3}{3} \right] G_s,
$$

$$
I_{y\phi} = -\frac{b^3}{12}(A_{11}^* h_b - B_{11}^*) + \left[\frac{t_s b^3}{12} h_t + \frac{h\, t_w^3}{12} e_s \right] E_s,
$$

$$
H_{x\phi} = -b(B_{13}^* C_b + D_{13}^*).
$$

EXTERNAL WORK

In a simply supported beam of span L, the external work is given by Sherbourne and Kabir [11], as a function of the internal bending moment:

$$W = \int_0^L M(z)(V'' - \phi U'')dz, \qquad (38)$$

where $M(z)$ represents the bending moment function. Now, with the external work from Equation 38 and the strain energy from Equation 24 or 37, the total potential energy is given by Equation 10.

I-BEAM UNDER POSITIVE END MOMENTS

For a simply supported beam, we take the Fourier series as shape functions of buckling deformations, which satisfy all boundary conditions:

$$\begin{Bmatrix} U \\ V \\ \phi \end{Bmatrix} = \sum_{n=1}^{\infty} \begin{Bmatrix} U_n \\ V_n \\ \phi_n \end{Bmatrix} \sin \frac{n\pi z}{L}. \qquad (39)$$

Thus, the strain energy for the beam with the bottom flange retrofitted only is:

$$U_i = \sum_{n=1}^{\infty} \left\{ \frac{n^4 \pi^4}{4L^3} \left[I_y U_n^2 + I_x V_n^2 \right. \right.$$
$$+ \left(I_\phi + \frac{L^2}{n^2 \pi^2} G \right) \phi_n^2 + 2 I_{y\phi} U_n \phi_n \right]$$
$$\left. - \sum_{m=1}^{\infty} \frac{8m\pi^2 n^3}{(n^2 - m^2)L^2} H_{x\phi} V_n \phi_m \right\}, \qquad (40)$$

where:

$$\sum_{m=1}^{\infty} \frac{8m\pi^2 n^3}{(n^2 - m^2)L^2} H_{x\phi} V_n \phi_m \rightarrow$$
$$\begin{cases} = 0 : (n + m) = \text{Even} \\ \neq 0 : (n + m) = \text{Odd} \end{cases}$$

For a simply supported beam under positive end moments, the Rayleigh-Ritz method thus gives the critical buckling moment for $n = 1$:

$$M_{ocr} = \frac{\pi^2}{L^2} I_{y\phi} \pm \frac{\pi}{L} \sqrt{I_y G \left(1 + \frac{\pi^2}{L^2} \frac{I_\phi}{G} \right)}, \qquad (41)$$

where:

$$I_y = \frac{b^3}{12}(A_{11}^* + t_s E_s),$$

$$I_\phi = \frac{b^3}{12}(A_{11}^* h_b^2 + E_s t_s h_t^2),$$

$$G = 4bD_{33}^* + \left[\frac{bt_s^3}{3} + \frac{ht_w^3}{3} \right] G_s,$$

$$I_{y\phi} = -\frac{b^3}{12}(A_{11}^* h_b - B_{11}^*) + \left[\frac{t_s b^3}{12} h_t + \frac{ht_w^3}{12} e_s \right] E_s.$$

Subsequently, for the case with both retrofitted flanges, $I_{y\phi} = 0$, the critical moment becomes:

$$M_{ocr} = \pm \frac{\pi}{L} \sqrt{I_y G \left(1 + \frac{\pi^2}{L^2} \frac{I_\phi}{G} \right)},$$

$$I_y = \frac{b^3}{6}(A_{11}^*),$$

$$I_\phi = \frac{b^3}{6}(A_{11}^* C^2),$$

$$G = 8bD_{33}^*. \qquad (42)$$

Similarly, for a both ends clamped I-beam, the following shape functions satisfy all boundary conditions as:

$$\begin{Bmatrix} U \\ V \\ \phi \end{Bmatrix} = \sum_{n=1}^{\infty} \begin{Bmatrix} U_n \\ V_n \\ \phi_n \end{Bmatrix} \sin \frac{\pi z}{L} \sin \frac{n\pi z}{L}. \qquad (43)$$

Inserting the introduced shape functions of Equation 43 into Equation 37, one can obtain:

$$M_{ocr} = \frac{\pi^2}{(kL)^2} I_{y\phi} \pm \frac{\pi}{kL} \sqrt{I_y G \left(1 + \frac{\pi^2}{(kL)^2} \frac{I_\phi}{G} \right)}, \qquad (44)$$

in which k is the effective length factor as below for the nth mode of buckling, and is equal to 0.5 for $n = 1$.

$$k^2 = \frac{1 + n^2}{1 + 6n^2 + n^4}. \qquad (45)$$

For a simply supported beam under unequal end moments, the bending moment diagram is a linear function through the beam and the shape modes consist of several terms in the Fourier series, so that $H_{x\phi}$ cannot be eliminated.

NUMERICAL RESULTS AND COMMENT

In this section, a parametric study was carried out for calculating the critical moment in a simple I-beam, as shown in Figure 9, for the case of TB under some traditional loading for both simple and clamped beams. It was also decided to extend the solution in a numerical analysis to make a comparison between mathematical manipulation and those results obtained by numerical modeling.
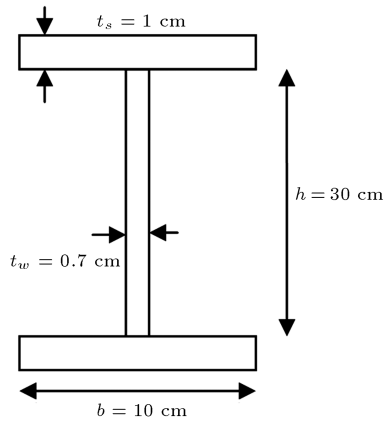
Figure 9. Steel I-beam, section dimensions.

An I-beam with length $L = 4000$ mm is considered in order to investigate the effects of FRP and its fiber orientation effect in lateral-torsional buckling capacity. The material properties for steel and FRP are assumed to be:

Steel:

$E_s = 200$ GPa, $v_s = 0.3$.

FRP:

$E_1 = 140$ GPa, $E_2 = 10$ GPa

$G_{12} = 5$ GPa, $v_{12} = 0.3$,

$t_F = 0.2$cm.

Figure 9 shows that the FEM model includes S8R elements provided for arbitrarily large rotations and small strains. S8R is a second-order element and is suitable for the analysis of composite and sandwich shells. To model hybrid elements consisting of steel-flange and FRP-laminates, a composite layup is used. Also, for applied end moments, Shell Edge Loads are used.

Figures 10 and 11 show variations of fiber angle, which is measured, with respect to the longitudinal axis of the beam in $[+\theta/ - \theta]$ laminate sequences versus percentage increase in the critical moment. It can be seen that for positive moment, the maximum and minimum of the buckling load are obtained by taking the fiber angles at $\theta = 0°$ and $\theta = 90°$, respectively. It is seen that at $\theta = 45°$ the numerical results are much closer to the analytical calculations owing to the effect of the $H_{x\phi}$ term, which is considered in numerical investigations. This term reflects the coupling effects between vertical and rotational deformations and is exited at $45°$. Therefore, it is expected to have a lower estimation in the buckling load capacity of the retrofitted beam.
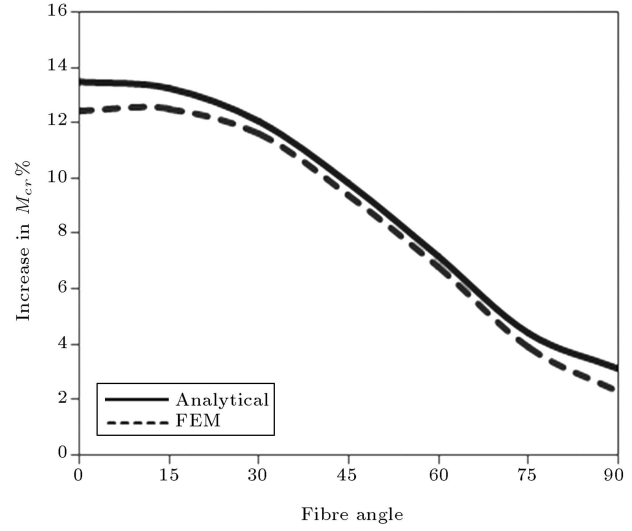

Figure 10. Comparison between analytical and FEM results for case TB under positive end moments.
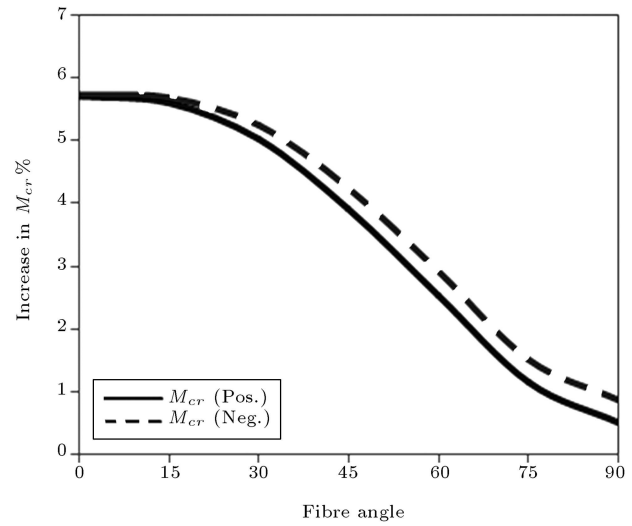

Figure 11. Comparison between analytical results of positive and negative critical moments for case BO under positive end moments.

According to the analytical solution, the maximum increases in critical moment are about 13.5% and 5.7% for cases of TB and BO.

The influence of fiber orientation on the critical end moment is depicted in Figure 11 for positive and negative end moments. The coupling moment of inertia, $I_{y\phi}$, is responsible for the detected differences at those angles not equal to zero and more pronounced for $\theta = 90°$.

Finally, Tables 2 to 4 represent a comparison between analytical and numerical results for sim55ple and clamped end beams for cases of TB. Incidentally, an I-beam like Figure 9, but with a thickness of 10mm for the web, was used for the clamped beam. Numerical results show that in both cases of simply supported

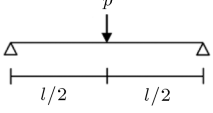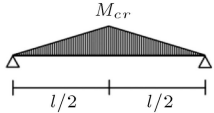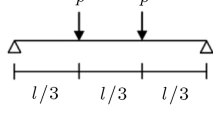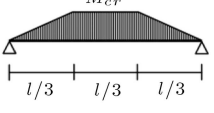**Table 2.** Critical load of some typically loaded beams as function of critical moment.
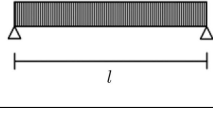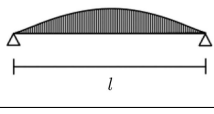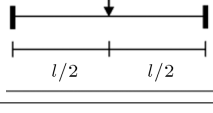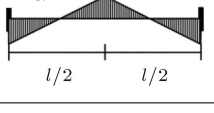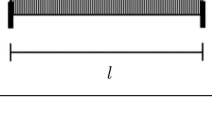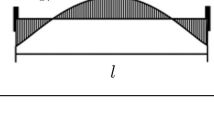
Beam ――――――― Critical Load	Load	Bending Moment Diagram
SS-1 ――――――― $p_{cr} = \frac{4 M_{cr}}{l}$		
SS-2 ――――――― $p_{cr} = \frac{3 M_{cr}}{l}$		
SS-3 ――――――― $q_{cr} = \frac{8 M_{cr}}{l^2}$		
CC-1 ――――――― $p_{cr} = \frac{8 M_{cr}}{l}$		
CC-2 ――――――― $q_{cr} = \frac{24 M_{cr}}{l^2}$		

Table 3. Increase in critical moment of case TB for typically loaded simple beam (%).

Angle	Beam SS-1		Beam SS-2		Beam SS-3	
	Analytical	FEM	Analytical	FEM	Analytical	FEM
0	12.90	11.39	12.90	11.23	14.81	14.04
15	12.65	11.69	12.65	11.50	14.55	13.78
30	11.53	11.47	11.55	11.21	13.44	12.67
45	9.62	9.96	9.64	9.65	11.51	10.75
60	7.39	7.57	7.41	7.25	9.24	8.50
75	5.24	4.77	5.25	4.46	7.04	6.32
90	4.27	3.34	4.27	3.05	6.04	5.33

and clamped end beams, distributed loading results of the analytical solution and FEM model are more in accordance than other loading.

CONCLUSION

This study exhibited how for a retrofitted I-beam using FRP sheets under a positive end moment, an analytical solution based on the energy method can give a critical value for the lateral-torsional buckling analysis. Based on the numerical results, using a thin layer of FRP sheet on the flanges of an I-beam can significantly develop the lateral-torsional buckling capacity of the beam. For the presented specimen, the FRP thickness

Table 4. Increase in critical moment of case TB for typically loaded clamped beam (%).

Angle	Beam CC-1		Beam CC-2	
	Analytical	FEM	Analytical	FEM
0	22.21	21.39	22.24	21.59
15	20.84	20.89	20.87	20.98
30	17.45	19.17	17.49	19.02
45	14.15	16.89	14.19	16.52
60	12.34	14.99	12.38	14.54
75	11.57	13.48	11.61	13.03
90	11.34	12.78	11.37	12.34

of which is one-fifth of the flange thickness, this development is about 13.5% and 5.7% in cases of using FRP at both flanges (TB) and the bottom flange only (BO), respectively. The parametric study with various fiber angles shows that the maximum and minimum increase in the buckling moment occurs at $\theta = 0°$ and $\theta = 90°$.

REFERENCES

1. Youssef, M.A. "Analytical prediction of the linear and nonlinear behaviour of steel beams rehabilitated using FRP sheets", *Engineering Structures*, **28**, pp. 903-911 (2006).

2. Phares, B.M. et al. "Strengthening of steel girder bridges using FRP", *MCTRS Proceedings*, Iowa State University, Ames, Iowa (2003).

3. EL Damatty, A.A. et al. "Rehabilitation of composite steel bridges using GFRP plates", *Applied Composite Materials*, **12**, pp. 309-325 (2005).

4. Qiao, P. et al. "Flexural–torsional buckling of fiber-reinforced plastic composite cantilever I-beams", *Composite Structures*, **60**, pp. 205-217 (2003).

5. Lee, J. and Lee, S. "Flexural-torsional behavior of thin-walled composite beams", *Thin-Walled Structures*, **42**, pp. 1293-1305 (2004).

6. Harries, K.A. et al. "Enhancing stability of structural steel sections using FRP", *Thin Walled Structures, Special Issue on FRP Strengthened Metallic Structures*, **47**, pp. 1092-1101 (2009).

7. Accord, N.B. and Earls, C.J. "Use of fiber reinforced polymer composite elements to enhance structural steel member ductility", *ASCE J. Comp. Constr.*, **10**, pp. 337-344 (2006).

8. Bazant, Z.P. and Cedolin, L. "Thin-walled beams", in *Stability of Structures: Elastic, Inelastic, Fracture and Damage Theories*, Dover Publication, Inc., Mineola, New York (2003).

9. Jons, R.M., *Mechanics of Composite Materials*, 2nd Ed., Taylor and Francis, Philadelphia, USA (1999).

10. Popov, I.P., *Engineering Mechanics of Solids*, ISBN 964-6904-14-6 (1961).

11. Sherbourne, A.N and Kabir, M.Z. "Shear strain effects in lateral-torsional strain of thin-walled fibrous composite beams", *Journal of Engineering Mechanics*, **121**, pp. 640-647 (1995).

BIOGRAPHIES

Mohammad Zaman Kabir is an Associate Professor in the Department of Civil and Environmental Engineering at Amirkabir University of Technology, Tehran, Iran from where he received his BS and MS degrees. He received his PhD from Waterloo University in Canada. His research interests include: Structural Stability, Structural Analysis using FEM, Experimental Methods in Structural Engineering, Composite Structures, Structural Optimization, Damage Detection and Rehabilitation of Structures.

Ali-Ehsan Seif is a MS Student in the Department of Civil and Environmental Engineering at Amirkabir University of Technology, Tehran, Iran. He received his BS degree from Imam-Hussein University. His MS Thesis is "Lateral-Torsional Buckling of Steel Beams using FRP sheets" and his research interests include: Structural Stability, Composite Retrofitting and Blast Loading of Structures.